Generation of 130 mW of 397.5 nm tunable laser via ring-cavity-enhanced frequency doubling

Yashuai Han, Xin Wen, Jiandong Bai, Baodong Yang, Yanhua Wang, Jun He, and Junmin Wang*

The State Key Laboratory of Quantum Optics and Quantum Optics Devices (Shanxi University), and Institute of Opto-Electronics, Shanxi University, 92 Wu Cheng Road, Tai Yuan 030006, Shan Xi Province, China

**Corresponding author: wwjjmm@sxu.edu.cn*

Received April 18, 2014; revised June 23, 2014; accepted June 23, 2014; posted June 24, 2014 (Doc. ID 210417); published 0 MONTH 0000

We report on the frequency doubling of a tapered amplifier-boosted distributed-Bragg-reflector continuous-wave laser system at 795 nm, using a PPKTP crystal placed in an external ring cavity. A tunable 397.5 nm violet laser power of 130 mW with a mode-matched input 795 nm laser power of 416 mW is obtained (conversion efficiency $\eta = 31\%$), limited by thermally induced bistability. However, when the violet laser is at the maximum output, a stable operation more than 30 min is hard to reach due to thermal effects. With a scanning cavity, the peak violet laser power rises up to 180 mW, corresponding to an overall efficiency of $\eta = 43\%$. The generated 397.5 nm laser with good beam quality and satisfying power has huge potential use in quantum optics and cold-atom physics.

OCIS codes: (190.2620) Harmonic generation and mixing; (140.2020) Diode lasers; (230.5750) Resonators.

http://dx.doi.org/10.1364/JOSAB.99.099999

1. INTRODUCTION

Compact high-power tunable violet laser sources are of interest for many scientific and technological applications, such as optical data storage, laser printing and lithography, spectroscopy, quantum optics, and cold-atom physics. The cooling and trapping of Ca^{+} ions, which play an important role in quantum manipulation and quantum computing areas, have been realized with a tunable 397 nm light source in several experiments [1–4]. Particularly, in the field of quantum optics, the major objective of the violet laser is the realization of the squeezed lights by pumping an optical parametric oscillator (OPO). The generated squeezing lights corresponding to the transitions of alkalis such as cesium (Cs) and rubidium (Rb) have great potential use, including in nonclassical spectroscopy [5], light–atom interaction [6,7], information storage and readout [8], quantum information networks [9], and ultraprecise measurement [10,11].

A universal approach to realize violet laser sources is second harmonic generation (SHG) of near-infrared light. However, this is limited by the absorption of nonlinear materials at violet wavelengths and associated thermal effects. Benefiting from the development of nonlinear crystals and low-loss coatings during the past decades, frequency doubling of Ti:sapphire lasers and tapered diode amplifiers has become an effective approach to realizing such violet lasers. For years, various nonlinear materials have been used. The potassium niobate ($KNbO_3$) crystal is widely used due to its large nonlinearity ($d_{\mathrm{eff}} \sim 18$ pm/V). In 1991, 650 mW of blue radiation at 430 nm was achieved with $KNbO_3$ in a ring cavity [12]. However, the phase-matching temperature for SHG of 795 nm is below the freezing point or above 100°C, which requires special precautions. What is more, the strong blue-induced infrared absorption (BLIIRA) at lower temperature renders it unsuitable for the generation of violet wavelengths. Another widely used material is lithium triborate (LBO) because of its wide transparent range (160–2600 nm). In 2008, using a LBO crystal in an external enhancement cavity, 1.1 W at 378 nm was generated, and the conversion efficiency was 35% [13]. Recently, 1 W at 399 nm has been obtained with a LBO crystal in a ring cavity, with an efficiency of 80% [14]. However, due to the low nonlinear coefficients ($d_{\mathrm{eff}} < 1$ pm/V), the SHG efficiency for LBO is sensitive to intra-cavity loss. Thus, it is unsuitable for the frequency conversion of low power sources, which requires a precise control of loss. Although a commercial LBO-based frequency doubler is available for the generation of violet light near 397 nm, the bad beam quality prevents it from pumping an OPO. Recently, quasi-phase-matched (QPM) materials such as PPLN and PPKTP have been available, which have the advantages of being free of walkoff, a convenient phase-matching scheme, and large effective nonlinearities ($d_{\mathrm{eff}}(\mathrm{PPLN}) \sim 17 - 18$ pm/V and $d_{\mathrm{eff}}(\mathrm{PPKTP}) \sim 7 - 9$ pm/V). For violet laser generation, PPKTP is superior to PPLN, which is resistant to photorefractive damage at room temperature. PPKTP has been used to generate 234 mW at 461 nm [15], 330 mW at 426 nm [16], and 318 mW at 404 nm [17] by means of external-cavity-enhanced SHG. In a recent paper, 340 mW blue light was generated with PPKTP by sum-frequency generation (SFG) between a tapered amplifier (TA) operated in a coupled cavity and a single-pass TA [18]. Compared with the method of SHG, the advantage of this approach is the tenability, which can easily be expanded to all the visible spectrum. However, this system is a little complicated with two TAs. Although many papers [8,9,19,20] mentioned the generation of 397.5 nm violet lasers by external-cavity SHG with PPKTP crystals, none of them presented a detailed study. In 2013, Zhai *et al.* [21] solely discussed the frequency doubling to 397 nm with PPKTP crystals in a ring cavity. However, they employed a tight focusing of the waist size to 25 μm in a 30 mm PPKTP crystal, resulting in severe thermal effects and low SHG power output (40 mW).

In the present work, we perform a detailed study on efficient 397.5 nm tunable violet light conversion from frequency doubling of a TA-boosted 795 nm distributed-Bragg-reflector (DBR) laser system with a PPKTP crystal in a ring cavity. Compared to the Ti:sapphire laser, our diode-based pump laser system is compact, inexpensive, and easy to operate. In general, the TA is seeded by an external-cavity diode laser (ECDL). Compared with this scheme, the DBR diode laser without external gratings is more compact and stable. By adjusting the temperature and injection current of the DBR laser, we are able to tune the wavelength of the laser and then address atomic transitions. When the laser is tuned to 793.676 nm, the SHG violet laser corresponds to a $^{40}Ca^{+}4S_{1/2}$–$4P_{1/2}$ transition, which can be applied in laser cooling and trapping of Ca^{+} ions. In this context, our group is engaged in the generation of polarization squeezed lights resonant with Rb D_1 transitions (795 nm), improving the signal-to-noise ratio (SNR) and sensitivity of the Rb-based SERF magnetometer and spin gyroscope by replacing the coherent probe laser. Based on this, the aim of our work is to achieve the violet laser at 397.5 nm with satisfying power and beam quality, which is suitable for pumping an OPO.

With the system, a maximum power of 130 mW at 397.5 nm is achieved with a mode-matched power of 416 mW, while in scanning mode this value rises up to 180 mW. When the violet laser is at the maximum output, the absorption of the violet laser leads to obvious thermal effects. As a consequence, a stable operation more than 30 min is hard to reach. We briefly discuss the thermally induced bistability and dephasing, which limit the efficiency and power stability in continuous-wave (cw) mode at high incident power. Finally, the beam profile and power stability of the generated violet light are presented.

2. SHG SETUP

A schematic drawing of the experimental setup is shown in Fig. 1. The pump laser is a TA-boosted 795 nm DBR diode laser. The DBR diode laser is TO-8 packaged, and the nominal linewidth and the maximum output power are ~1 MHz and 180 mW at 795 nm, respectively. A 30 dB optical isolator is adopted between the DBR laser and TA to prevent the optical feedback into the DBR laser. An electro-optical modulator (EOM) carried with a 4.1 MHz radio frequency provides phase modulation of the pump beam to lock the enhancement cavity by using the Pound–Drever–Hall modulation sideband method. A rotatable polarization beam splitter (PBS) cube placed in front of the TA is used to obtain the correct polarization input. The system provides a single-longitudinal-mode power $P_{\omega} = 500$ mW at 795 nm.

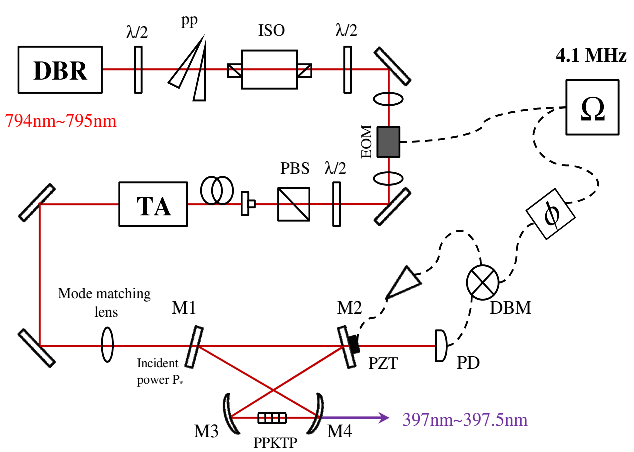

Fig. 1. Schematic of the experimental setup. DBR, distributed Bragg reflection diode laser; PP, plastic prism; TA, tapered amplifier; DBM, double-balanced mixer.

The enhancement cavity is designed in a symmetric bow-tie ring configuration with a folding angle of 8°, which leads to a negligible astigmatism. A lens mode matches the pump beam into the enhancement cavity. The cavity is made of two plane mirrors (M1 and M2) and two curved mirrors (M3 and M4) with radius of curvature of 100 mm. The mirrors are highly reflecting at the fundamental wave (FW) wavelength, except for the input coupler M1 with a power transmission T_1 between 11.7% and 7.4%. In addition, M4 has a power transmission of 94% at the SHG wavelength. The back faces of all mirrors are antireflection (AR) coated at the two wavelengths. M2 is mounted on a piezoelectric transducer (PZT) for the electronic locking of the enhancement cavity.

A 20-mm-long PPKTP (Raicol Crystal Ltd.) crystal with a poling period of 3.15 μm is placed at the waist between the curved mirrors (see Fig. 1). According to the theory proposed by Boyd and Kleinman [22], the optimum confocal condition for an incident Gaussian beam and the desired beam waist are related to the crystal length. They defined the focusing parameters $\xi = L/b$, where L is the length of PPKTP crystal and $b = \pi\omega_0^2/\lambda$. The optimum focusing condition is found to be $\xi = 2.84$, which results in an optimal waist of 22 μm in our case. However, as the SHG wavelength is approaching the limit of the transparency window of KTP (350 nm), the linear absorption becomes an important issue. Earlier reports [19–21] have shown considerable absorption in the violet wavelength with KTP, leading to large thermal effects. Based on this, we deliberately avoid optimal focusing to circumvent these thermal effects. Weak focusing on the crystal can efficiently weaken the thermal effects and still achieve considerable conversion efficiency. This also ensures an increased crystal lifetime. Based on this, we design the cavity with a total length of 60 cm and a distance of 12 cm between curved mirrors. This results in a waist of 40 μm, which is nearly two times as large as the optimal size. The crystal is placed in a copper-made oven, whose temperature is controlled by a thermoelectric Peltier element. The crystal Z axis is matched with the direction of electric-field polarization of the TA laser, and no extra $\lambda/2$ plate is needed. The generated SH beam is transmitted through M4 as shown in Fig. 1. The SHG beam is separated from the nonconverted FW beam with a dichroic mirror.

3. EXPERIMENTAL RESULTS AND DISCUSSION

Scanning the injection current of the DFB laser, we obtain the saturation absorption spectroscopy (SAS) of D_1 transitions of Rb^{85} and Rb^{87} atoms, shown in Fig. 2. It is indicated that the 795 nm laser can be tuned continuously around 8.5 GHz. Thus, the 397.5 nm violet laser can also be continuously tuned based on the tunable range of the 795 nm laser. We can lock the laser

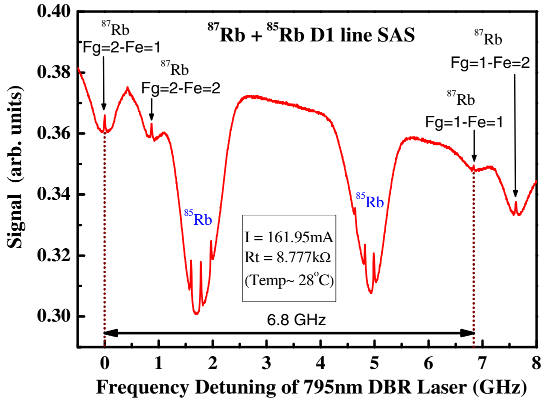

Fig. 2. Saturation absorption spectroscopy (SAS) of D_1 transitions of Rb^{85} and Rb^{87} atoms obtained by the 795 nm DBR laser.

frequency to any of D_1 transitions of Rb^{85} and Rb^{87} atoms, which enables the 397.5 nm laser stabilization.

The single-pass conversion efficiency E_{NL} of the PPKTP crystal is measured by removing the input coupler (M1) and detecting the generated SHG power transmitting through M4, which preserves the focusing condition used in the actual resonant cavity. By varying the crystal temperature and hence the phase matching, the temperature tuning curve is measured, shown in Fig. 3(a). We perform the measurement at an incident FW power of 100 mW in order to avoid unwanted contributions from thermal effects. 160 μW of SHG power is generated at the phase temperature of 50.5°C, resulting in $E_{NL} = 1.6\%/\mathrm{W}$. The full-width at half maximum (FWHM) bandwidth is 0.5°C. The measured temperature tuning curve is in good agreement with sinc^2 fitting in Fig. 3(a), implying good homogeneity of the refractive index at lower power levels.

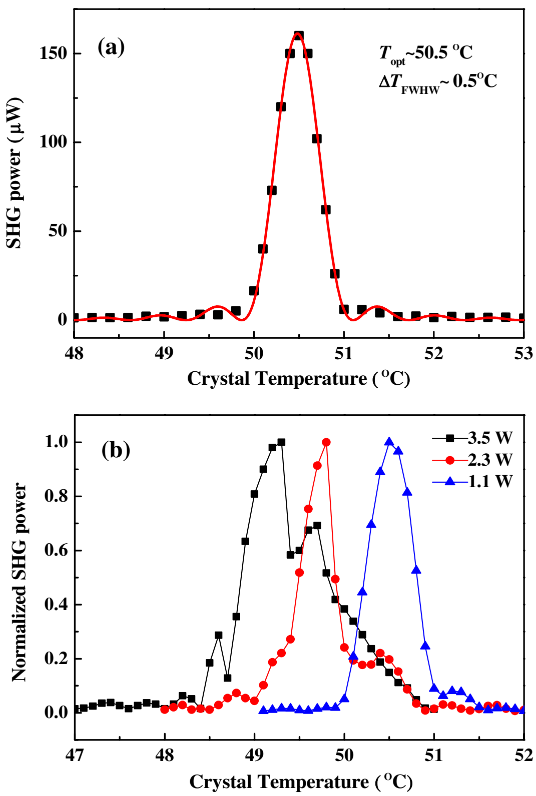

Fig. 3. (a) Measured temperature tuning curve with sinc^2 fitting in single-pass configuration. The pump power is 100 mW. The temperature bandwidth from the fitting curve is $\Delta T_{\mathrm{FWHM}} = 0.5°\mathrm{C}$. (b) Temperature tuning curve for cavity configuration. The incident powers are ~100 mW, ~250 mW, and ~450 mW, corresponding to the intracavity circulating powers of ~1.1 W, ~2.3 W, and ~3.5 W, respectively.

We also measure the temperature tuning curve for the cavity configuration with incident power of ~100 mW, ~250 mW, and ~450 mW, corresponding to the intra-cavity power of ~1.1 W, ~2.3 W, and ~3.5 W, respectively. The temperatures of phase-matching peaks are 50.5, 49.8, and 49.3°C, respectively, shown in Fig. 3(b). At lower incident power, the temperature tuning curve and the phase-matching temperature stay the same compared with the single-pass configuration. However, at higher incident FW power, the phase-matching peak shifts towards lower temperature. As the SHG wavelength is approaching the limit of the transparency window of KTP (350 nm), the significantly increased absorption of the circulating FW power and especially the SHG power at high power level lead to heating of the crystal. This thermal effect induces a thermal gradient larger than the crystal thermal acceptance. As a result, the oven temperature has to be lower to compensate the temperature rise in the crystal. This is proved by results shown in Fig. 3(b). In addition, we find that the phase-matching curve deviates from the sinc^2 function at higher power. This might be attributed to the inhomogeneous temperature distribution in the crystal caused by light-induced absorption.

The SHG power versus mode-matched FW power can be written as [15,16]

$$\sqrt{\eta}\left[2-\sqrt{1-T_1}\left(2-L-\Gamma\sqrt{\frac{\eta P_1}{E_{NL}}}\right)\right]^2-4T_1\sqrt{E_{NL}P_1}=0, \tag{1}$$

where $\eta = P_2/P_1$ is the overall conversion efficiency, P_1 is the mode-matched fundamental power, and P_2 is the generated SHG power. Γ includes all nonlinear losses and can be written as $\Gamma = E_{NL} + \Gamma_{\mathrm{abs}}$. Γ_{abs} formulates the SH light absorption inside the crystal: $P_{\mathrm{abs}} = \Gamma_{\mathrm{abs}} P_c^2$. The absorption in the blue region is in the range of 10%–20%/cm [15,16,23]. As for 397.5 nm, it might be larger. L is the total round-trip loss in the cavity except for the transmission T_1 of input coupler M1, which is due to absorption and scattering of crystal and cavity mirrors. The intra-cavity loss is measured to be 4.5%.

To achieve a high SHG efficiency, optical impedance matching must be considered. The choice of input coupler depends on the total losses including linear and nonlinear losses. The optimal transmission T_1 of the input coupler yields [15,16]

$$T_1^{opt} = \frac{L}{2} + \sqrt{\left(\frac{L}{2}\right)^2 + \Gamma P_1}. \tag{2}$$

Based on the parameters ($L = 4.5\%$, $E_{NL} = 1.6\%/\mathrm{W}$, $\Gamma_{\mathrm{abs}} = 0.22 E_{NL}$, and $P_1 = 0.42$ W) of our cavity, the optimal T_1^{opt} is calculated 11.6%. The comparisons for two different transmissions (11.7% and 7.4%) are shown in Fig. 4. We conclude that the 11.7% transmission approaches the optimal

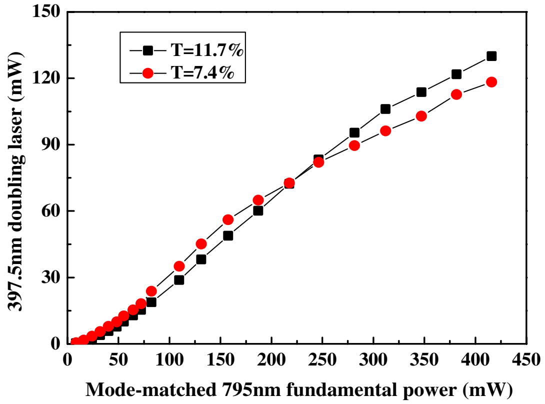

Fig. 4. 397.5 nm doubling power versus the mode-matched fundamental power under two different input couplers (11.7% and 7.4%). The black squares correspond to $T_1 = 11.7\%$, and the red dots correspond to $T_1 = 7.4\%$.

value, leading to an excellent perfect impedance matching and a higher SHG efficiency.

The generated 397.5 nm doubling power and conversion efficiency versus the mode-matched fundamental power in cw and scanning mode with 11.7% transmission of the input coupler are plotted in Fig. 5. The spatial profile of the output beam

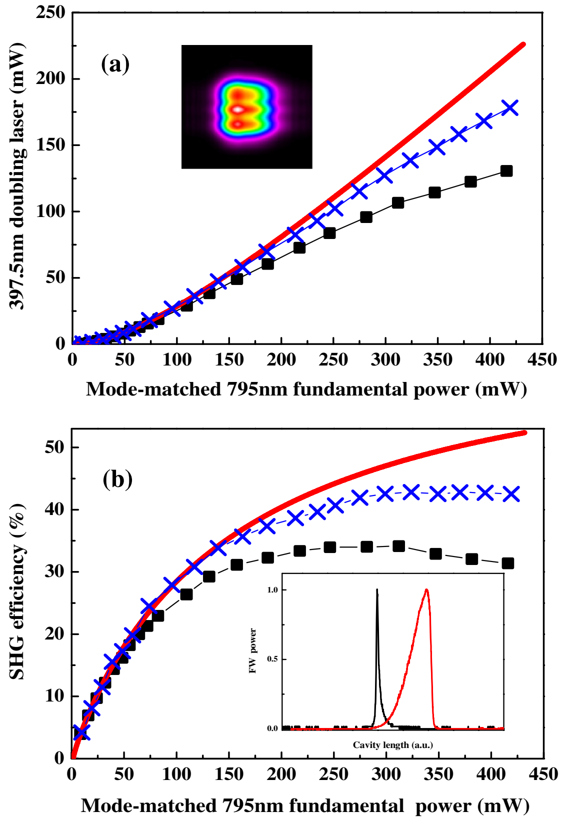

Fig. 5. (a) 397.5 nm doubling power P_2 and (b) conversion efficiency η as a function of mode-matched fundamental power P_1 with 11.7% transmission of input coupler. Solid lines are the theoretically calculated results on parameters ($E_{NL} = 1.6\%/\mathrm{W}$, $L = 4.5\%$, $T_1 = 11.7\%$, and $\Gamma_{\mathrm{abs}} = 0.22E_{NL}$), black squares represent results in cw mode, and blue crosses represent peak power in scanning mode. The inset of (a) shows the spatial profile of the output beam from the TA. The inset of (b) shows the fringe asymmetry observed on the FW fringe when scanning the PZT (red line, contracting cavity length; black line, expanding length).

from the TA is far from a Gaussian beam shown in the inset of Fig. 5(a), resulting in a typical mode-matching efficiency of 80%. The temperature is carefully optimized to give the maximum SHG output for each data point. The measured SHG power and conversion efficiency in scanning mode are in good agreement with the theoretical calculation from Eq. (1) with parameters ($E_{NL} = 1.6\%/\mathrm{W}$, $L = 4.5\%$, $T_1 = 11.7\%$, and $\Gamma_{\mathrm{abs}} = 0.22E_{NL}$) until $P_1 = 300$ mW. After this value, slight deviation is seen as the pump power increases. This is due to the less accurate evaluation of the mode-matched power in this range. The transverse beam of the TA becomes worse gradually with the injection current of the TA increasing. As a result, the mode-matched power drops at high power range. The cw results deviate from the scanning results for mode-matching power larger than 150 mW, which can be attributed to the increased difficulty in locking the cavity. The inset of Fig. 5(b) shows the fringe asymmetry observed on the FW fringe when scanning the PZT of the enhancement cavity. First consider the case in which the PZT is expanding and therefore the cavity is shortening (red line). As the cavity is tuned to be resonant with the FW laser, the circulating FW power and especially the SHG power become increasingly important, leading to heating of the crystal. The absorption causes a rise in crystal temperature, thus resulting in an increase of the optical path length due to the positive value for dn/dT at the FW wavelength. This lengthening of the optical length induced by thermal effects is in the opposite direction to the scanning. Before the peak of the resonance is reached, this thermal effect slows down the shortening of the cavity length. Therefore, the point of the cavity resonance shifts to a shorter cavity length, which results in a slow increase of the circulating FW power. This is the self-stabilizing effect of the optical path to the laser frequency [15]. Once resonance is reached, the thermal effect decreases and the cavity makes an abrupt transition out of resonance. For the case in which the cavity is lengthening (black line), the thermal effect accelerates the lengthening of the cavity length. Therefore, the cavity sweeps rapidly through resonance. This thermally induced bistability prevents locking of the cavity to the top of the distorted fringe in cw mode, leading to a deviation from the results in the scanning mode.

The wavelength of the 397.5 nm laser can be tuned by changing the wavelength of the 795 nm laser and simultaneously changing the PPKTP temperature to assure phase matching. By tuning the 795 nm laser from 794.278 to 795.382 nm, we have tuned the violet laser in the 397.139–397.691 range. The corresponding phase-matching temperature changes from 38.3 to 57.5°C. In this way, the obtained power is indeed affected. Meanwhile, we have measured the continuously tunable range of the violet laser. By tuning the 795 nm laser continuously, the generated 397.5 nm laser can be tuned continuously. The generated 397.5 nm laser passes through a confocal Fabry–Perot (FP) cavity with a cavity length of 25 mm. When the 795 nm DBR laser is tuned by scanning the current of the DBR laser with a speed of 5.4 GHz/s, the FP trace of 397.5 nm is shown in the Fig. 6. It is noticed that the cavity length is not scanned. The scanning speed is limited by the bandwidth of the cavity feedback loop. We can infer from the figure that the 397.5 nm laser can be tuned continuously around 3 GHz without losing the lock of the cavity. The continuously tunable range is limited by

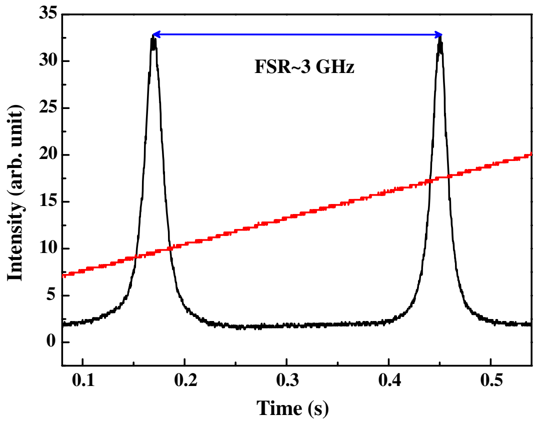

Fig. 6. Confocal FP cavity trace of 397.5 nm laser when the 795 nm laser is tuned.

the maximum deforming length of the PZT. It is also indicated that the violet laser at 397.5 nm is single-frequency.

The output power stability at 397.5 nm is measured at various fundamental powers for 30 min in cw mode, shown in Fig. 7(a). The RMS fluctuations range from 0.7% at 100 mW to 1.5% at 250 mW of mode-matched FW power, indicating good power stability. However, the degradation of the SHG power is observed when the mode-matched power approaches 420 mW, resulting in a large RMS fluctuation of 3.5%. This degradation is largely attributed to thermally induced dephasing [24] caused by absorption at FW and especially SHG wavelengths in PPKTP crystal when it is operated at high power density levels. We restrict the violet power to 80 mW to minimize this thermal effect. Operating in the region can also minimize the thermally induced bistability, allowing for a stable locking of the enhancement cavity. The beam quality M^2 values and beam profile are shown in Fig. 7(b). The measured M^2 values for both axes are $M_x^2 = 1.19$ (3) and $M_y^2 = 1.16$ (3). The transverse intensity distribution for both axes is in good agreement with Gaussian fitting.

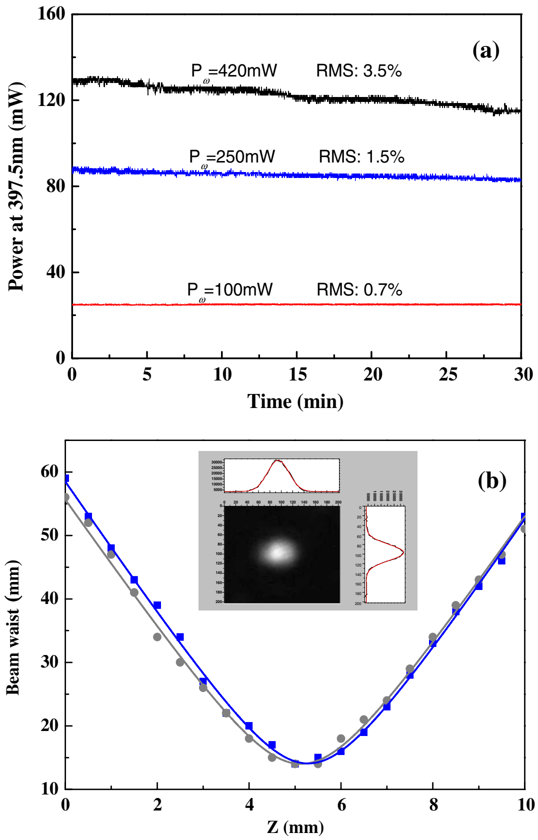

Fig. 7. (a) Power stability over 30 min at various fundamental power levels. (b) Beam quality M^2 values of SHG beam for both axes at maximum violet power. The blue squares are results for the x axis, and the gray dots are results for the y axis. The inset is the beam profile of the SHW beam.

4. CONCLUSION

We have demonstrated the generation of 130 mW of cw power at 397.5 nm from frequency doubling of a TA-boosted DBR laser system with a PPKTP crystal in a ring cavity. When the cavity is operated in scanning mode, the violet power rises up to 180 mW with a mode-matched power of 416 mW, corresponding to an overall efficiency of $\eta = 43\%$. The power stability and beam quality at 397.5 nm are measured to be good in cw mode. The stable and tunable violet laser source with a satisfying power and good beam quality paves the way to the realization of the squeezed light at 795 nm, which is resonant with the rubidium D_1 line and the cooling and trapping of Ca^+ ions.

Compared with Refs. [15–17], our SHG efficiency is lower. This can be attributed to two reasons. For one, as our SHG wavelength is shorter approaching the limit of the transparency window of KTP (350 nm), the absorption at the FW and SHG wavelengths is larger. Although the waist size is nearly two times as large as the optimal size, thermally induced bistability and dephasing are observed, which limit the efficiency at high incident power in cw mode. Also, the thermal effects change the eigenmode of the cavity, resulting in a different mode matching. For the other, imperfect optical quality and coatings of cavity mirrors and crystal faces together with the absorption of the crystal at the FW wavelength result in a higher intra-cavity loss of 4.5%. Further improvements in efficiency can be obtained by reducing loss in the following aspects. First, the scattering loss can be reduced by using super polished mirrors. Second, the reflecting loss can be lowered by using the ion beam sputter coating technology for all four cavity mirrors. Third, the intra-cavity loss can be further reduced by a semimonolithic [25] or monolithic [26] cavity configuration. After the loss is reduced, one needs to optimize the input coupler to match with the total loss of the cavity. With these approaches, we believe the efficiency can be improved dramatically.

ACKNOWLEDGMENTS

This project is supported by the National Natural Science Foundation of China (grant nos. 61227902, 11274213, 61205215, and 11104172), the National Major Scientific Research Program of China (grant no. 2012CB921601), and the Project for Excellent Research Team from the National Natural Science Foundation of China (grant No. 61121064).

REFERENCES

1. S. Urabe, M. Watanabe, H. Imajo, and K. Hayasaka, "Laser cooling of trapped Ca^+ and measurement of the $3^2D_{5/2}$ state lifetime," Opt. Lett. **17**, 1140–1142 (1992).
2. G. P. T. Lancaster, H. Häffner, M. A. Wilson, C. Becher, J. Eschner, F. Schmidt-kaler, and R. Blatt, "Doppler cooling a

single Ca^+ ion with a violet extended-cavity diode laser," Appl. Phys. B **76**, 805–808 (2003).

3. H. Guan, B. Guo, G. Huang, H. Shu, X. Huang, and K. Gao, "Stabilization of 397 nm and 866 nm external cavity diode lasers for cooling a single calcium ion," Opt. Commun. **274**, 182–186 (2007).
4. N. M. Linke, C. J. Balance, and D. M. Lucas, "Injection locking of two frequency-doubled lasers with 3.2 GHz offset for driving Raman transitions with low photo scattering in $^{43}Ca^+$," Opt. Lett. **38**, 5087–5089 (2013).
5. E. S. Polzik, J. Carri, and H. J. Kimble, "Spectroscopy with squeezed light," Phys. Rev. Lett. **68**, 3020–3023 (1992).
6. J. Hald, J. L. Sørensen, C. Schori, and E. S. Polzik, "Spin squeezed atoms: a macroscopic entangled ensemble created by light," Phys. Rev. Lett. **83**, 1319–1322 (1999).
7. Q. A. Turchette, N. P. Georgiades, C. J. Hood, H. J. Kimble, and A. S. Parkins, "Squeezed excitation in cavity QED: experiment and theory," Phys. Rev. A **58**, 4056–4077 (1998).
8. J. Appel, E. Figueroa, D. Korystov, M. Lobino, and A. I. Lvovsky, "Quantum memory for squeezed light," Phys. Rev. Lett. **100**, 093602 (2008).
9. X. Jia, Z. Yan, Z. Duan, X. Su, H. Wang, C. Xie, and K. Peng, "Experimental realization of three-color entanglement at optical fiber communication and atomic storage wavelengths," Phys. Rev. Lett. **109**, 253604 (2012).
10. F. Wolfgramm, A. Cerè, F. A. Beduini, A. Predojević, M. Koschorreck, and M. W. Mitchell, "Squeezed-light optical magnetometer," Phys. Rev. Lett. **105**, 053601 (2010).
11. T. Eberle, S. Steinlechner, J. Bauchrowitz, V. Händchen, H. Vahlbruch, M. Mehmet, H. Müller-Ebhardt, and R. Schnabel, "Quantum enhancement of the zero-area Sagnac interferometer topology for gravitational wave detection," Phys. Rev. Lett. **104**, 251102 (2010).
12. E. S. Polzik and H. J. Kimble, "Frequency doubling with $KNbO_3$ in an external cavity," Opt. Lett. **16**, 1400–1402 (1991).
13. Y. H. Cha, K. H. Ko, G. Lim, J. M. Han, H. M. Park, T. S. Kim, and D. Y. Jeong, "External-cavity frequency doubling of a 5-W 756-nm injecton-locked Ti:sapphire laser," Opt. Express **16**, 4866–4871 (2008).
14. M. Pizzocaro, D. Calonico, P. C. Pastor, J. Catani, G. A. Costanzo, F. Levi, and L. Lorini, "Efficient frequency doubling at 399 nm," arXiv:1401.1623 (2014).
15. R. L. Targat, J.-J. Zondy, and P. Lemonde, "75%-efficiency blue generation from an intracavity PPKTP frequency doubler," Opt. Commun. **247**, 471–481 (2005).
16. F. Villa, A. Chiummo, E. Giacobino, and A. Bramati, "High-efficiency blue-light generation with a ring cavity with periodically poled KTP," J. Opt. Soc. Am. B **24**, 576–580 (2007).
17. J. H. Lundeman, O. B. Jensen, P. E. Andersen, S. Andersson-Engels, B. Sumpf, G. Erbert, and P. M. Petersen, "High power 404 nm source based on second harmonic generation in PPKTP of a tapered external feedback diode laser," Opt. Express **16**, 2486–2493 (2008).
18. O. B. Jensen and P. M. Petersen, "Single-frequency blue light generation by single-pass sum-frequency generation in a coupled ring cavity tapered laser, " Appl. Phys. Lett **103**, 141107 (2013).
19. T. Tanimura, D. Akamatsu, Y. Yokoi, A. Furusawa, and M. Kozuma, "Generation of a squeezed vacuum resonant on a rubidium D1 line with periodically poled $KTiOPO_4$," Opt. Lett. **31**, 2344–2346 (2006).
20. G. Hétet, O. Glöckl, K. A. Pilypas, C. C. Harb, B. C. Buchler, H.-A. Bachor, and P. K. Lam, "Squeezed light for bandwidth-limited atom optics experiments at the rubidium D1 line," J. Phys. B **40**, 221–226 (2007).
21. Y. Zhai, B. Fan, S. Yang, Y. Zhang, X. Qi, X. Zhou, and X. Chen, "A tunable blue source with narrow linewidth for cold atom experiments," Chin. Phys. Lett. **30**, 044209 (2013).
22. G. D. Boyd and D. A. Kleinman, "Parametric interaction of focused Gaussian light beams," J. Appl. Phys. **39**, 3597–3639 (1968).
23. G. Hansson, H. Karlsson, S. Wang, and F. Laurell, "Transmission measurements in KTP and isomorphic compounds," Appl. Opt. **39**, 5058–5069 (2000).
24. Z. M. Liao, S. A. Payne, J. Dawson, A. Drobshoff, C. Ebbers, and D. Pennington, "Thermally induced dephasing in periodically poled KTP frequency-doubling crystals," J. Opt. Soc. Am. B **21**, 2191–2196 (2004).
25. S. Ast, R. M. Nia, A. Schönbeck, N. Lastzka, J. Steinlechner, T. Eberle, M. Mehmet, S. Steinlechner, and R. Schnabel, "High-efficiency frequency doubling of continuous-wave laser light," Opt. Lett. **36**, 3467–3469 (2011).
26. X. Deng, J. Zhang, Y. C. Zhang, G. Li, and T. C. Zhang, "Generation of blue light at 426 nm by frequency doubling with a monolithic periodically poled $KTiOPO_4$," Opt. Express **21**, 25907–25911 (2013).

Queries

1. AU: AR and PZT defined correctly?